*Computers & Structures* Vol. 32, No. 3/4, pp. 797–814, 1989
Printed in Great Britain.

0045-7949/89 $3.00 + 0.00


# THE MITC7 AND MITC9 PLATE BENDING ELEMENTS

KLAUS-JÜRGEN BATHE,† FRANCO BREZZI‡ and SEONG WOOK CHO†
†Massachusetts Institute of Technology, Cambridge, MA 02139, U.S.A.
‡Università di Pavia, I.A.N. del C.N.R., 27100 Pavia, Italy

**Abstract**—We present in this paper two plate bending elements that have been proposed and mathematically analyzed previously by Bathe, Brezzi and Fortin: the MITC7 (a triangular) element and the MITC9 (a quadrilateral) element. The formulation of these elements is summarized and example solutions are given that demonstrate the high accuracy of these elements.

## 1. INTRODUCTION

Although much research effort has been spent on the development of reliable and efficient plate and shell elements, there is still a large interest in arriving at improved elements. During the recent years we have concentrated on the development of elements based on Mixed-Interpolated Tensorial Components (i.e. our MITC elements) and have proposed the 4-node MITC4 element [1, 2], the 8-node MITC8 element [3] and a complete family of new elements [4, 5]. The 4-node and 8-node elements have been developed for general shell analysis and are available in ADINA [6], whereas the elements given in [4, 5] have so far only been proposed for plate analysis, but have excellent potential to be extended for applicability to effective general shell analysis as well.

We mentioned before [2, 3] that the extension of a plate element to a general (linear and nonlinear) shell element usually represents a major step and is frequently not possible. It is therefore most appropriate to concentrate directly on the development of general nonlinear shell analysis capabilities which can then also be used in the linear analysis of plates. Hence, we have emphasized in our work the development of general shell elements and proposed the MITC4 and MITC8 elements.

To understand the behavior of these elements and possibly to design additional elements, we conducted mathematical analyses which were, however, so far only possible for the case of the linear analysis of plates. These theoretical considerations led us to some interesting and quite general results, which are in essence based on an analogy that can be drawn between the analysis of incompressible media and the analysis of Reissner–Mindlin plate problems. The mathematical analyses also identified additional elements for the plate bending problem and since these elements are constructed much like the MITC4 and MITC8 elements, we can be quite confident that they can be extended to general shell analysis as well.

The objective in this paper is to summarize the formulation of two of the new elements for the plate bending problem and present a numerical evaluation. The elements considered are a 7-node triangular element, the MITC7 element, and a 9-node quadrilateral element, the MITC9 element. Both these elements pass the patch test, they contain no spurious zero energy mode and, as demonstrated in the paper, have excellent predictive capability.

## 2. THE PLATE BENDING PROBLEM CONSIDERED

We consider the spaces: $\Theta = (H_0^1(\Omega))^2$ and $W = H_0^1(\Omega)$ and a load function $f$ given in $L^2(\Omega)$. The sequence of problems under consideration is:

$$P_t: \inf_{\theta\in\Theta,\, w\in W} \frac{t^3}{2} a(\theta, \theta) + \frac{\lambda t}{2} \| \theta - \nabla w \|_0^2 - t^3(f, w)$$

where $(t^3/2)a(\theta, \theta)$ is the bending internal energy, and $(\lambda t/2)\| \theta - \nabla w \|_0^2$ is the shear energy. $\| \ \|_0$ and $( \ , \ )$ represent respectively the norm and the inner product in $L^2(\Omega)$.

Assume now that we are given the finite element subspaces $\Theta_h \subset \Theta$ and $W_h \subset W$. The corresponding discretized problem is described by

$$\tilde{P}_{th}: \inf_{\theta_h\in\Theta_h,\, w_h\in W_h} \frac{t^3}{2} a(\theta_h, \theta_h) + \frac{\lambda t}{2} \| \theta_h - \nabla w_h \|_0^2 - t^3(f, w_h).$$

In general, $\tilde{P}_{th}$ 'locks' for small $t$. A common procedure is to reduce the influence of the shear energy. We consider here the case in which the reduction is carried out in the following way: we assume that we are given a third finite element space, $\Gamma_h$, and a linear operator $R$ which takes values in $\Gamma_h$. Then we use $\| R(\theta_h - \nabla w_h) \|_0^2$ instead of $\| \theta_h - \nabla w_h \|_0^2$ in the shear energy. In our formulation we further assume that

$$R\nabla w_h = \nabla w_h \quad \text{for all } w_h \in W_h \tag{1}$$

so that the discretized problem takes its final form

$$P_{th}: \inf_{\theta_h \in \Theta_h,\, w_h \in W_h} \frac{t^3}{2} a(\theta_h, \theta_h) + \frac{\lambda t}{2} \| R\theta_h - \nabla w_h \|_0^2 - t^3(f, w_h).$$

Setting

$$\gamma = \lambda t^{-2}(\theta - \nabla w) \quad \text{and} \quad \gamma_h = \lambda t^{-2}(R\theta_h - \nabla w_h) \tag{2}$$

the Euler equations of $P_t$ and $P_{th}$ are, respectively

$$a(\theta, \eta) + (\gamma, \eta - \nabla\zeta) = (f, \zeta) \quad \forall \eta \in \Theta, \forall \zeta \in W$$
$$\gamma = \lambda t^{-2}(\theta - \nabla w) \tag{3}$$

and

$$a(\theta_h, \eta) + (\gamma_h, R\eta - \nabla\zeta) = (f, \zeta) \quad \forall \eta \in \Theta_h, \forall \zeta \in W_h$$
$$\gamma_h = \lambda t^{-2}(R\theta_h - \nabla w_h). \tag{4}$$

We may note that the limit problems are

$$a(\theta, \eta) + (\gamma, \eta - \nabla\zeta) = (f, \zeta) \quad \forall \eta \in \Theta, \forall \zeta \in W$$
$$\theta = \nabla w \tag{5}$$

and

$$a(\theta_h, \eta) + (\gamma_h, R\eta - \nabla\zeta) = (f, \zeta) \quad \forall \eta \in \Theta_h, \forall \zeta \in W_h$$
$$R\theta_h = \nabla w_h. \tag{6}$$

*Remark* 1: The limit problems in (5) and (6) were analyzed in [4, 5]. Such analysis is therefore not complete, yet gives valuable insight into the behavior of element formulations when applied to the analysis of very thin plates.

*Remark* 2: It is not difficult to show that (5) and (6) are the limit problems of (3) and (4) respectively (see for instance [7]). In particular the limit $w$ will be the solution corresponding to the Kirchhoff model. Note also that the limit $\gamma_h$ that appears in (6) will still belong to $R(\Theta_h) - \nabla(W_h)$. Although we are not studying the convergence of $\gamma_h$ to $\gamma$, the results given in [8], with the discussion below, give some insight into the behavior of $\gamma_h$.

*Remark* 3: The operator $R$ defines the 'tying' to be employed between the basis functions used in $\Gamma_h$ and the functions used in $W_h$ and $\Theta_h$.

## 3. THE FINITE ELEMENT DISCRETIZATIONS

Following the discussion of the previous section, a finite element discretization is characterized by the choice of the finite element spaces $\Theta_h$, $W_h$, $\Gamma_h$ and by the choice of the linear operator $R$. Note that these choices are not independent of each other. We introduce below the two choices of specific interest in this paper, i.e. the MITC7 and MITC9 elements, but also briefly summarize the MITC4 element construction (see Fig. 1). The MITC4 element formulation is only included to indicate the similarity in the three element formulations. We should also mention that in this section we assume uniform decompositions, a restriction which we remove in Sec. 5.

### 3.1. *The MITC4 element*

For the four-node element [1, 2] we use

$$\Theta_h = \{\eta \mid \eta \in (H_0^1(\Omega))^2, \quad \eta|_K \in (Q_1)^2 \, \forall K\} \tag{7}$$

$$W_h = \{\zeta \mid \zeta \in H_0^1(\Omega), \quad \zeta|_K \in Q_1 \, \forall K\} \tag{8}$$

where $Q_1$ is the set of polynomials of degree $\leqslant 1$ in each variable and $K$ is the current element in the discretization. The space $\Gamma_h$ is given by

$$\Gamma_h = \{\delta \mid \delta|_K \in TR(K) \, \forall K, \delta \cdot \tau \text{ continuous at the interelement boundaries}\} \tag{9}$$

where $\tau$ is the tangential unit vector to each edge of the element and

$$TR(K) = \{\delta \mid \delta_1 = a_1 + b_1 y, \delta_2 = a_2 + b_2 x\} \tag{10}$$

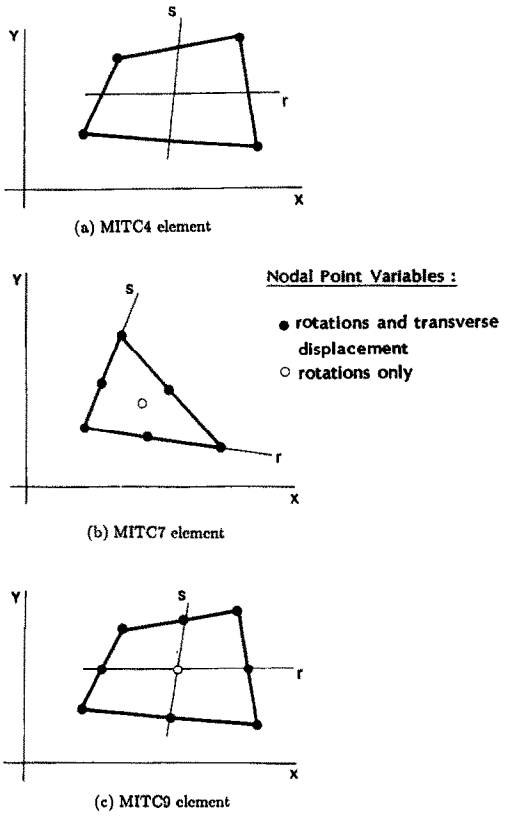


(a) MITC4 element

(b) MITC7 element

(c) MITC9 element

Fig. 1. Plate bending elements considered.

is a sort of 'rotated Raviart–Thomas' space of order zero [9]. We next introduce the reduction operator $R$ by describing its action on the current element: for $\boldsymbol{\eta}$ smooth in $K$, $R\boldsymbol{\eta}|_K$ is the unique element in $TR(K)$ that satisfies

$$\int_e (\boldsymbol{\eta} - R\boldsymbol{\eta}) \cdot \boldsymbol{\tau}\, ds = 0 \quad \text{for all edges } e \text{ of } K. \tag{11}$$

Note that if $\boldsymbol{\eta} \in (Q_1)^2$ then (11) is satisfied if and only if $\boldsymbol{\eta} \cdot \boldsymbol{\tau} = R(\boldsymbol{\eta}) \cdot \boldsymbol{\tau}$ at the midpoints of each edge.

### 3.2. *The MITC7 element*

For the 7-node triangular elements [5] we use

$$\boldsymbol{\Theta}_h = \{\boldsymbol{\eta} \mid \boldsymbol{\eta} \in (H_0^1)^2, \quad \boldsymbol{\eta}|_T \in (S_7(T))^2 \, \forall T\} \tag{12}$$

$$W_h = \{\zeta \mid \zeta \in H_0^1, \quad \zeta|_T \in P_2 \, \forall T\} \tag{13}$$

where $T$ is the triangular element in the discretization, $P_2$ is the space of complete second order polynomials (corresponding to a 6-node element), and $S_7$ is

$$S_7(T) = \{\varphi \mid \varphi \in P_3, \varphi|_e \in P_2 \text{ on each edge } e \text{ of } T\}. \tag{14}$$

Clearly $S_7$ is a finite dimensional linear space of dimension 7. It can also be characterized as $S_7 = P_2 \oplus \{\lambda_1\lambda_2\lambda_3\}$ where $\lambda_1\lambda_2\lambda_3$ is the cubic bubble in $T$. As degrees of freedom in $S_7(T)$ we can clearly choose the values at the vertices, at the midpoint of the edges and at the barycenter of $T$.

We also set, in each triangle $T$,

$$TR_1(T) = \{\boldsymbol{\delta} \mid \delta_1 = a_1 + b_1 x + c_1 y + y(\mathrm{d}x + ey);$$

$$\delta_2 = a_2 + b_2 x + c_2 y - x(\mathrm{d}x + ey)\}. \tag{15}$$

The space $TR_1(T)$ is a kind of 'rotated Raviart–Thomas' space of order one [9]. The space $\boldsymbol{\Gamma}_h$ is given by

$$\boldsymbol{\Gamma}_h = \{\boldsymbol{\delta} \mid \boldsymbol{\delta}|_T \in TR_1(T), \forall T, \boldsymbol{\delta} \cdot \boldsymbol{\tau} \text{ continuous at the interelement boundaries, } \boldsymbol{\delta} \cdot \boldsymbol{\tau} = 0 \text{ on } \partial\Omega\} \tag{16}$$

where $\boldsymbol{\tau}$ is the tangential unit vector to each edge of each element.

We next introduce the reduction operator $R$. Its action on the current element is given as follows: for $\boldsymbol{\eta}$ smooth in $T$, $R\boldsymbol{\eta}$ in $T$ is the unique element in $TR_1(T)$ that satisfies

$$\int_e (\boldsymbol{\eta} - R\boldsymbol{\eta}) \cdot \boldsymbol{\tau} p_1(s)\, ds = 0 \quad \forall e \text{ edge of } T, \quad \forall p_1(s) \in P_1(e) \tag{17}$$

$$\int_T (\boldsymbol{\eta} - R\boldsymbol{\eta})\, \mathrm{d}x\, \mathrm{d}y = \mathbf{0}. \tag{18}$$

It is easy to see that (17) and (18) characterize $R\boldsymbol{\eta}$ in $T$ in a unique way. It is also clear that if $\boldsymbol{\eta}$ is continuous in $\Omega$, then the $R\boldsymbol{\eta}$ constructed element by element through (17) and (18) actually belongs to $\boldsymbol{\Gamma}_h$ [because (17) ensures the continuity of $(R\boldsymbol{\eta}) \cdot \boldsymbol{\tau}$ at the interelement boundaries].

### 3.3. *The MITC9 element*

For the 9-node element [4, 5] we use

$$\boldsymbol{\Theta}_h = \{\boldsymbol{\eta} \mid \boldsymbol{\eta} \in (H_0^1(\Omega))^2, \quad \boldsymbol{\eta}|_K \in (Q_2)^2 \, \forall K\} \tag{19}$$

$$W_h = \{\zeta \mid \zeta \in H_0^1(\Omega), \quad \zeta|_K \in Q_2^* \, \forall K\} \tag{20}$$

where $Q_2$ is the space of polynomials of degree $\leqslant 2$ in each variable (corresponding to a 9-node element) and $Q_2^*$ is its usual serendipity reduction (corresponding to an 8-node element). In order to introduce the space $\boldsymbol{\Gamma}_h$ we define first the space of polynomials

$$G = \{\boldsymbol{\delta} \mid \delta_1 = a_1 + b_1 x + c_1 y + d_1 xy + e_1 y^2;$$

$$\delta_2 = a_2 + b_2 x + c_2 y + d_2 xy + e_2 x^2\} \tag{21}$$

which is some kind of rotated Brezzi–Douglas–Fortin–Marini space [10]. Note that if $\zeta \in Q_2^*$ then $\nabla\zeta \in G$. This is the main reason why $W_h$ has been discretized with the interpolations of the 8-node element instead of the 9-node element. We introduce now the space $\boldsymbol{\Gamma}_h$:

$$\boldsymbol{\Gamma}_h = \{\boldsymbol{\delta} \mid \boldsymbol{\delta}|_K \in G \, \forall K, \boldsymbol{\delta} \cdot \boldsymbol{\tau} \text{ continuous at the interelement boundaries, } \boldsymbol{\delta} \cdot \boldsymbol{\tau} = 0 \text{ on } \partial\Omega\}. \tag{22}$$

Further, we define the action of the reduction operator $R$ on the current element $K$ in the following way: for $\boldsymbol{\eta}$ smooth in $K$, $R\boldsymbol{\eta}|_K$ is the unique element in $G$ that satisfies

$$\int_e (\boldsymbol{\eta} - R\boldsymbol{\eta}) \cdot \boldsymbol{\tau} p_1(s)\, ds = 0 \quad \forall e \text{ edge of } K, \quad \forall p_1(s) \text{ polynomial of degree } \leqslant 1 \text{ on } e \tag{23}$$

$$\int_K (\boldsymbol{\eta} - R\boldsymbol{\eta})\, \mathrm{d}x\, \mathrm{d}y = \mathbf{0}. \tag{24}$$

Note that if $\boldsymbol{\eta} \in (Q_2)^2$ then (23) holds if and only if $\boldsymbol{\eta} \cdot \boldsymbol{\tau} = (R\boldsymbol{\eta}) \cdot \boldsymbol{\tau}$ at the two Gauss points of each edge.

## 4. A BRIEF SUMMARY OF THE ERROR ANALYSIS—UNIFORM DECOMPOSITIONS

Our analysis of the above elements depends to a large extent on the theoretical results already available for finite element solutions of the response of incompressible media. A key step is that we are looking for a 'pressure space' $Q_h$ made of discontinu-

ous finite element functions† such that, for all $\boldsymbol{\eta} \in \boldsymbol{\Theta}_h$, we have

$$(\text{rot}\,\boldsymbol{\eta}, q_h) = (\text{rot}(R\boldsymbol{\eta}), q_h) \quad \forall q_h \in Q_h \tag{25}$$

where

$$\text{rot}\,\boldsymbol{\eta} \equiv (\partial\eta_2/\partial x) - (\partial\eta_1/\partial y),$$

and

$$\text{rot}(\boldsymbol{\Gamma}_h) \subseteq Q_h. \tag{26}$$

Conditions (25) and (26) are related to the so-called 'commuting diagram property' of Douglas and Roberts [11] that is used in the study of mixed methods for elliptic equations. It is easy to check that (25) and (26) hold if we take for the MITC4 element

$$Q_h = \{q \mid q|_K \in P_0 \,\forall K\} \tag{27}$$

and for the MITC7 and MITC9 elements

$$Q_h = \{q \mid q|_{K/T} \in P_1 \,\forall K/T\}. \tag{28}$$

In both cases $P_k$ denotes the set of polynomials of total degree $\leqslant k$: hence $Q_h$ has local dimension 1 in the MITC4 case and dimension 3 in the MITC7 and MITC9 cases. Note that the relation (25) is satisfied because of the specific operator $R$ used for each of the elements.

In order to analyze the error between $\boldsymbol{\theta}$ and $\boldsymbol{\theta}_h$ in (5) and (6) (and as a consequence the error between $w$ and $w_h$) we want to build a pair $\hat{\boldsymbol{\theta}}, \hat{w}$ in $\boldsymbol{\Theta}_h \times W_h$ such that $\|\boldsymbol{\theta} - \hat{\boldsymbol{\theta}}\|_1$ is optimally small and

$$R\hat{\boldsymbol{\theta}} = \nabla\hat{w}. \tag{29}$$

Condition (29) implies

$$\text{rot}\,R\hat{\boldsymbol{\theta}} = 0 \tag{30}$$

which, in its turn, using (25) and (26) is equivalent to

$$(\text{rot}\,\hat{\boldsymbol{\theta}}, q_h) = 0 \quad \forall q_h \in Q_h. \tag{31}$$

Hence, a possible way of constructing $\hat{\boldsymbol{\theta}}$ is as follows. For $\boldsymbol{\theta}$ given in $(H_0^1(\Omega))^2$ and satisfying $\text{rot}\,\boldsymbol{\theta} = 0$, consider the following problem:

find

$$\boldsymbol{\beta}, p \in \boldsymbol{\Theta} \times L^2(\Omega)$$

such that

$$a(\boldsymbol{\beta}, \boldsymbol{\eta}) + (p, \text{rot}\,\boldsymbol{\eta}) = a(\boldsymbol{\theta}, \boldsymbol{\eta}) \quad \forall \boldsymbol{\eta} \in \boldsymbol{\Theta} \tag{32}$$

$$(q, \text{rot}\,\boldsymbol{\beta}) = 0 \quad \forall q \in L^2(\Omega)$$

and its approximation,

find

$$\hat{\boldsymbol{\theta}}, p_h \in \boldsymbol{\Theta}_h \times Q_h$$

such that

$$a(\hat{\boldsymbol{\theta}}, \boldsymbol{\eta}) + (p_h, \text{rot}\,\boldsymbol{\eta}) = a(\boldsymbol{\theta}, \boldsymbol{\eta}) \quad \forall \boldsymbol{\eta} \in \boldsymbol{\Theta}_h \tag{33}$$

$$(q, \text{rot}\,\hat{\boldsymbol{\theta}}) = 0 \quad \forall q \in Q_h.$$

Note that (32) is a kind of Stokes problem and its solution is given by $\boldsymbol{\beta} = \boldsymbol{\theta}, p = 0$. If the pair $\boldsymbol{\Theta}_h, Q_h$ used in (33) is a suitable finite element discretization for the Stokes problem one might expect to have optimal error bounds for $\hat{\boldsymbol{\theta}} - \boldsymbol{\theta}$. For the MITC4 element the pair $\boldsymbol{\Theta}_h, Q_h$ is the classical bilinear velocities–constant pressure (or $Q_1$–$P_0$) element, and we know that

$$\|\boldsymbol{\theta} - \hat{\boldsymbol{\theta}}\|_1 \leqslant c\,h\,\|\boldsymbol{\theta}\|_2. \tag{34}$$

For the MITC7 element the pair $\boldsymbol{\Theta}_h, Q_h$ is the Crouzeix–Raviart element with the velocities given by quadratic plus cubic bubble variations and the pressure given by linear variation. In the case of the MITC9 element the pair $\boldsymbol{\Theta}_h, Q_h$ is the biquadratic velocities and linear pressure (the $Q_2$–$P_1$) element, and for both these elements we know

$$\|\boldsymbol{\theta} - \hat{\boldsymbol{\theta}}\|_1 \leqslant c\,h^2\|\boldsymbol{\theta}\|_3. \tag{35}$$

Note on the other hand that once $\hat{\boldsymbol{\theta}}$ satisfying (30) has been found, then we can uniquely determine the $\hat{w} \in W$ that satisfies (29). It is easy to check that in our two cases such a $\hat{w}$ is an element of $W_h$.

In [4, 5, 7] we have analyzed the solutions to be expected and obtained the following detailed error estimates: for the MITC4 element,

$$\|\boldsymbol{\theta} - \boldsymbol{\theta}_h\|_1 + \|\nabla w - \nabla w_h\|_0 \leqslant c\,h(\|\boldsymbol{\theta}\|_2 + \|\boldsymbol{\gamma}\|_0) \tag{36}$$

and for the MITC7 and MITC9 elements,

$$\|\boldsymbol{\theta} - \boldsymbol{\theta}_h\|_1 + \|\nabla w - \nabla w_h\|_0 \leqslant c\,h^2(\|\boldsymbol{\theta}\|_3 + \|\boldsymbol{\gamma}\|_1). \tag{37}$$

Hence the MITC4 element shows linear convergence behavior whereas the MITC7 and MITC9 elements show quadratic convergence. This result corresponds to the behavior of the $Q_1$–$P_0$ and $Q_2$–$P_1$ elements, respectively [12], and we can anticipate an excellent predictive capability of the MITC7 and MITC9 elements.

† This space corresponds to the pressure space in incompressible solutions.

## 5. GENERALIZATION OF ELEMENTS TO NONUNIFORM DECOMPOSITIONS

If the elements are to be useful in practice, it is important that they are formulated for general geometries. The MITC4 and MITC9 elements must correspond to general quadrilateral elements and the MITC7 element should correspond to a general triangle.

To generalize the formulations given in Sec. 3, we interpolate the covariant strains as defined in $\Gamma_h$ as a function of the natural coordinate systems $r, s$. Hence, with the strain tensors given as

$$\boldsymbol{\varepsilon} = \tilde{\varepsilon}_{ij}\mathbf{g}^i\mathbf{g}^j \tag{38}$$

where $i$ and $j$ permute over $r, s, t$, we use for the MITC4 element [1, 2]

$$\tilde{\varepsilon}_{rt} = a_1 + b_1 s \tag{39}$$

$$\tilde{\varepsilon}_{st} = a_2 + b_2 r \tag{40}$$

and for the MITC7 element

$$\tilde{\varepsilon}_{rt} = a_1 + b_1 r + c_1 s + s(dr + es) \tag{41}$$

$$\tilde{\varepsilon}_{st} = a_2 + b_2 r + c_2 s - r(dr + es) \tag{42}$$

and finally for the MITC9 element

$$\tilde{\varepsilon}_{rt} = a_1 + b_1 r + c_1 s + d_1 rs + e_1 s^2 \tag{43}$$

$$\tilde{\varepsilon}_{st} = a_2 + b_2 r + c_2 s + d_2 rs + e_2 r^2. \tag{44}$$

The contravariant base vectors $\mathbf{g}^i$ in (38) are of course calculated from the covariant base vectors $\mathbf{g}_i$, where, for example, $\mathbf{g}_r = \partial\mathbf{x}/\partial r$, $\mathbf{x}^T = [x, y, z]$. Note that only the transverse shear strain components are defined by the separate interpolations whereas the bending strains are obtained directly from the assumptions for the section rotations in $\boldsymbol{\Theta}_h$. The use of (38) with the $\tilde{\varepsilon}_{rt}$ and $\tilde{\varepsilon}_{st}$ interpolations employed for the MITC4 element has been described in detail in [2], and we proceed in the same way for the MITC7 and MITC9 elements.

There is, however, one additional consideration; namely the MITC7 and MITC9 element formulations involve the tying of the covariant shear strain components at the Gauss points on the edges *and* by an integral over the element domains, whereas the MITC4 element formulation only involves tying at the midpoints of the element edges. This integral-tying requires some additional computations when compared to simple point-tying and it is reasonable to ask whether instead of the integration, a point-tying at a certain point in the interior of the element may yield the same numerical accuracy in solutions. An interior point-tying was also used and

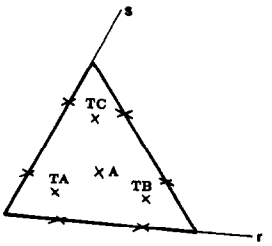


(a) Tying for MITC7 element:

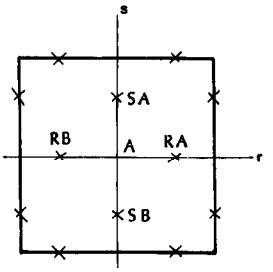


(b) Tying for MITC9 element:

Fig. 2. Gauss points used for tying of covariant shear strain components.

was shown to be effective in the formulation of the MITC8 element [3].

As reported in detail in the next section, the numerical results show that indeed the following point-tying is effective.

—For the MITC7 element, we use instead of the integral-tying given by (18), simply the mean of the values at points *TA*, *TB* and *TC* of the element; hence eqn (18) is replaced by [see Fig. 2(a)],

$$\tfrac{1}{3}(\boldsymbol{\eta}|_{TA} + \boldsymbol{\eta}|_{TB} + \boldsymbol{\eta}|_{TC}) = R\boldsymbol{\eta}|_A. \tag{45}$$

—For the MITC9 element, we use instead of the integral-tying given by (24), simply the mean of the values at points *RA*, *RB* and *SA*, *SB*, respectively [see Fig. 2(b)],

$$\tfrac{1}{2}(\eta_1|_{RA} + \eta_1|_{RB}) = R\eta_1|_A$$

$$\tfrac{1}{2}(\eta_2|_{SA} + \eta_2|_{SB}) = R\eta_2|_A. \tag{46}$$

In summary, for the MITC7 element we use the six Gauss points along the element sides and the Gauss points *TA*, *TB* and *TC* to express the eight constants in (41) and (42) in terms of the covariant strain components directly evaluated from the displacement/rotation interpolations. For the MITC9 element we use the eight Gauss points along the element sides and the mean of the values at the Gauss points *RA*, *RB* and *SA*, *SB*, respectively, to express the 10

constants in (43) and (44) in terms of the covariant strain components directly evaluated from the displacement/rotation interpolations. The details of such evaluation are given in [2].

In the next section we show numerical results obtained with the use of the integral-tying and the point-tying summarized above. Using the integral-tying we have the elements MITC7′ and MITC9′ whereas we refer to the elements MITC7 and MITC9 when using the point-tying. Here we should note that for rectangular element geometries, the elements MITC9 and MITC9′ are identical, hence our analysis given in Sec. 3 is totally applicable even when using the point-tying. However, we cannot make such observation regarding the MITC7 and MITC7′ elements, although the numerical results using these elements show small differences.

## 6. NUMERICAL RESULTS

The objective in this section is to present some numerical results of plate analyses obtained using the MITC7 and MITC9 elements. These results demonstrate the excellent predictive capabilities of the elements.

We also present some comparisons with results obtained with the MITC4 [2] and MITC8 [3] elements. Note that the MITC7 element stiffness matrix is evaluated using 6-point Gauss numerical integration and the MITC9 element is evaluated using $3 \times 3$ Gauss numerical integration and that these elements (and the MITC4 and MITC8 elements) do not contain any spurious zero energy modes.

### 6.1. *Patch test*

Figure 3 shows the patch of elements considered. As usual, when we test whether the patch test is passed, we only delete the minimum number of degrees of freedom to eliminate the physical rigid body modes [1]. We recall that the MITC4 and MITC8 elements pass the patch test.

The MITC7 and MITC9 elements pass the patch test. Further, it is interesting to note that the MITC7′ element also passes the patch test, whereas the MITC9′ element does not pass the test, but the degree of failure is not severe. Figure 4 shows the stress distributions obtained when the patch of MITC9′ elements is subjected to a constant bending moment. We observe that the predicted stresses do not vary from the analytical solution by a large amount.

Although this simple patch test does not display the complete convergence characteristics of an element, the test does show the sensitivity of an element to geometric distortions, and a condition for a reliable element is that it should satisfy (or at least almost satisfy) the test [3].

### 6.2. *Analysis of a square plate*

Figure 5 shows the plate problems considered and the meshes used in the analyses. Table 1 summarizes

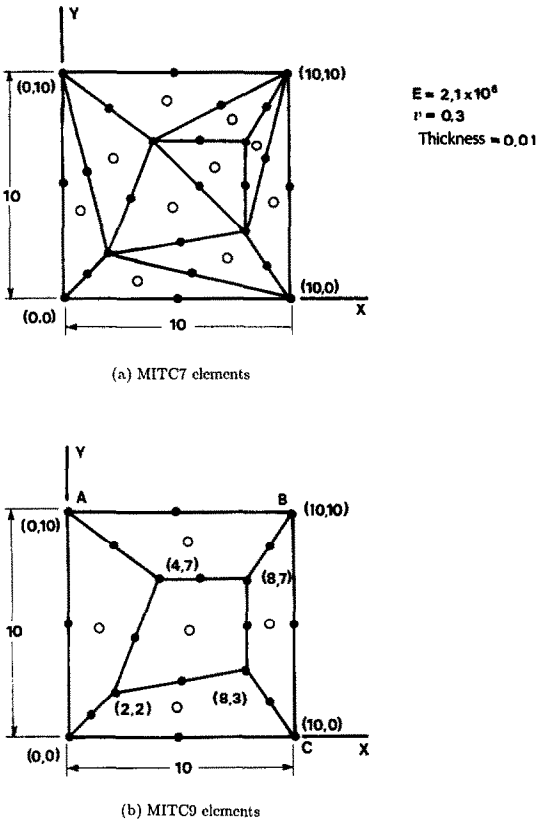


Fig. 3. Patch of elements considered.

the displacement results obtained, including those using the MITC4 and MITC8 elements. Figure 6 shows displacement and stress distributions calculated using the MITC7 and MITC9 elements with a comparison to the analytical solution [13].

The stresses have been calculated at the nodal points from the element displacements and hence stress jumps can be observed. However, the stress jumps are small for the fine mesh results and are largely confined to the area of the stress singularity (the center of the plate when subjected to the concentrated load).

Note that in these analyses, the finite element imposed boundary conditions correspond to the 'soft' conditions for the problem considered [14].

The meshes distort-1 and distort-2 have of course only been included in the tests in order to identify the distortion sensitivity of the elements [3].

Considering these results we note the excellent predictive capabilities of the MITC7 and MITC9 elements, and that there is little difference between the results of the MITC7′ and MITC7 elements, and the MITC9′ and MITC9 elements, respectively.

### 6.3. *Analysis of a circular plate*

Figure 7 shows the circular plate problem considered and the meshes used. Table 2 compares the displacement results obtained and Fig. 8 shows dis-

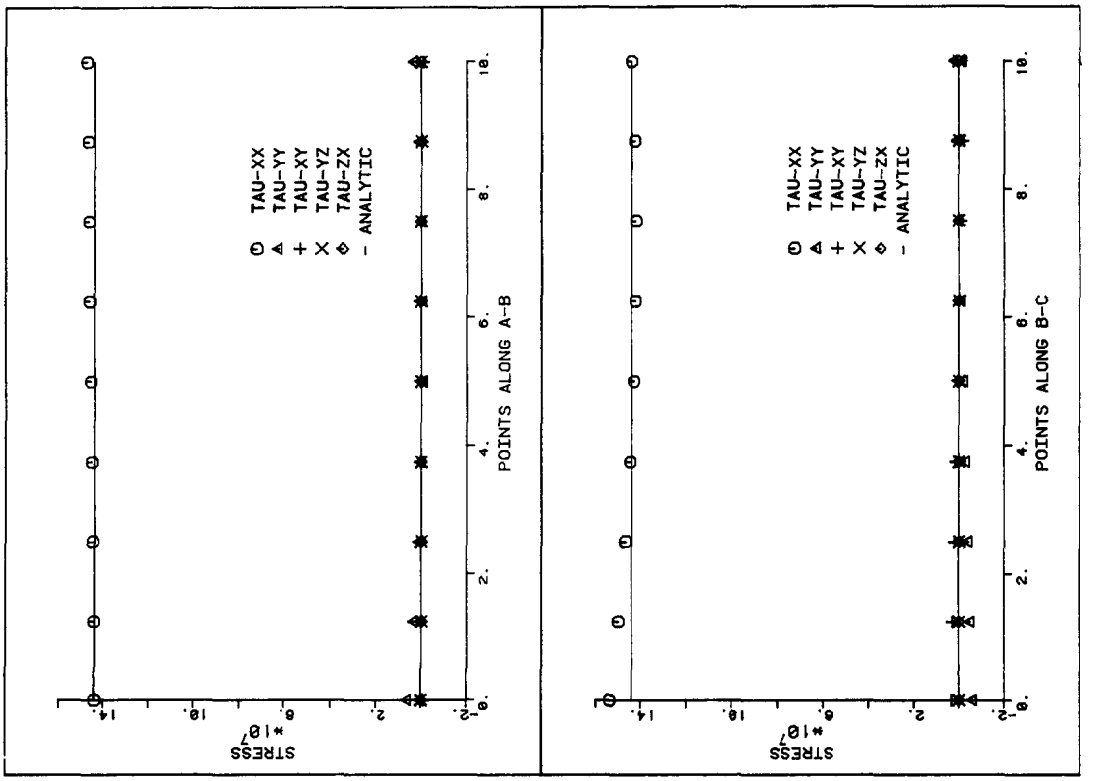


Fig. 4. Stress distributions in the patch using MITC9′ elements.

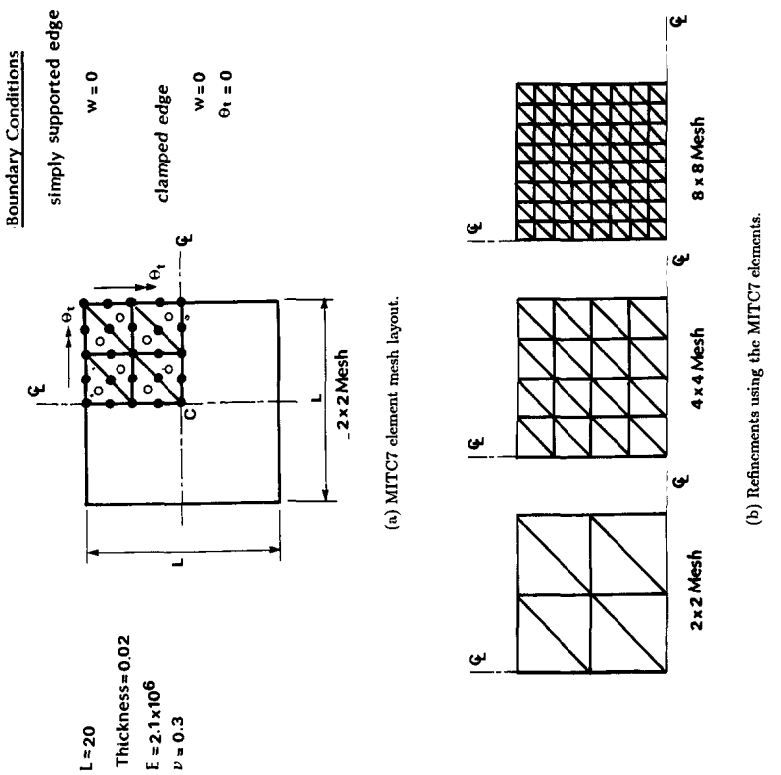


(a) MITC7 element mesh layout.

(b) Refinements using the MITC7 elements.

Fig. 5(a, b)

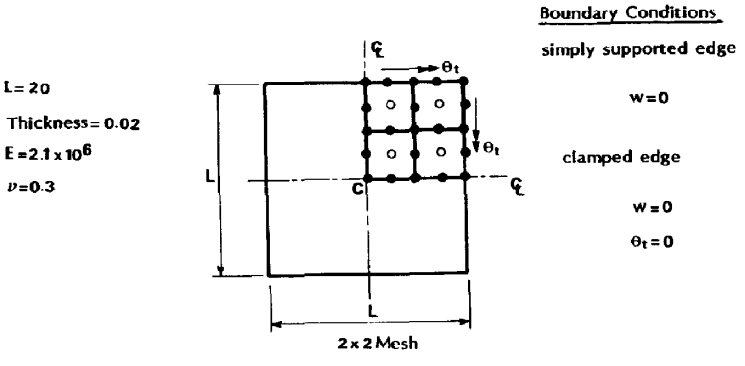


(c) MITC9 element mesh layout.

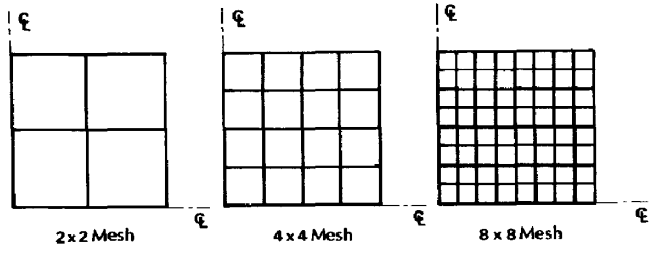


(d) Refinements using the MITC9 elements.

Fig. 5(c, d)

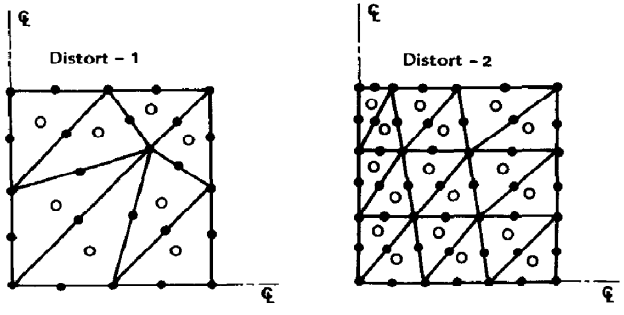


(e) Distorted mesh layout for MITC7 elements.
The element distortions are shown to scale.

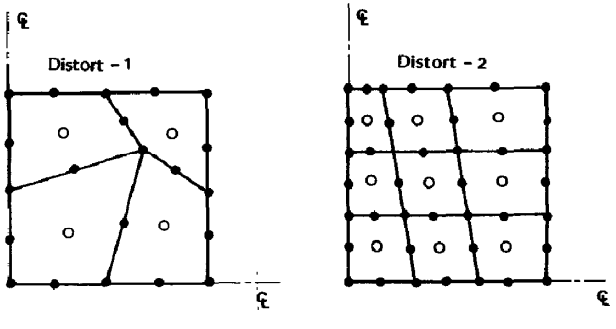


(f) Distorted mesh layout for MITC9 elements.
The element distortions are shown to scale.

Fig. 5(e, f). Analysis of a square plate.

Table 1. Analysis of a square plate. The analytical solution used as reference is the Kirchhoff plate theory solution [13]. (a) Response for various plate thicknesses for concentrated load at the center of the plate, $2 \times 2$ mesh

| Element | Thickness | $\alpha$†: simply supported edge | $\alpha$: clamped edge |
|---|---|---|---|
| MITC4 | 0.2 | 0.996 | 0.869 |
| | 0.02 | 0.995 | 0.867 |
| | 0.002 | 0.995 | 0.867 |
| MITC8 | 0.2 | 1.000 | 1.004 |
| | 0.02 | 0.998 | 1.001 |
| | 0.002 | 0.998 | 1.001 |
| MITC7′ | 0.2 | 0.982 | 0.918 |
| | 0.02 | 0.980 | 0.907 |
| | 0.002 | 0.980 | 0.907 |
| MITC9′ | 0.2 | 1.000 | 1.010 |
| | 0.02 | 0.998 | 1.006 |
| | 0.002 | 0.998 | 1.006 |
| MITC7 | 0.2 | 0.982 | 0.929 |
| | 0.02 | 0.979 | 0.918 |
| | 0.002 | 0.979 | 0.918 |
| MITC9 | 0.2 | 1.000 | 1.010 |
| | 0.02 | 0.998 | 1.006 |
| | 0.002 | 0.998 | 1.006 |

(b) Response for various mesh layouts (thickness = 0.02)

| | | Concentrated load | | Uniform pressure | |
|---|---|---|---|---|---|
| Element | Mesh | $\alpha$: simply supported edge | $\alpha$: clamped edge | $\alpha$: simply supported edge | $\alpha$: clamped edge |
| MITC4 | $2 \times 2$ | 0.995 | 0.867 | 0.981 | 0.963 |
| | $4 \times 4$ | 0.995 | 0.965 | 0.996 | 0.993 |
| | $8 \times 8$ | 0.998 | 0.992 | 0.999 | 1.001 |
| MITC8 | $2 \times 2$ | 0.998 | 1.001 | 1.000 | 1.006 |
| | $4 \times 4$ | 1.000 | 1.001 | 1.001 | 1.005 |
| | $8 \times 8$ | 1.000 | 1.002 | 1.001 | 1.004 |
| MITC7′ | $2 \times 2$ | 0.980 | 0.907 | 1.003 | 0.965 |
| | $4 \times 4$ | 0.994 | 0.985 | 1.000 | 1.001 |
| | $8 \times 8$ | 0.999 | 0.999 | 1.000 | 1.004 |
| MITC9′ | $2 \times 2$ | 0.998 | 1.006 | 0.999 | 1.025 |
| | $4 \times 4$ | 1.000 | 1.001 | 1.000 | 1.005 |
| | $8 \times 8$ | 1.000 | 1.002 | 1.000 | 1.004 |
| MITC7 | $2 \times 2$ | 0.979 | 0.918 | 1.003 | 0.977 |
| | $4 \times 4$ | 0.994 | 0.987 | 1.001 | 1.003 |
| | $8 \times 8$ | 0.999 | 0.999 | 1.000 | 1.004 |
| MITC9 | $2 \times 2$ | 0.998 | 1.006 | 0.999 | 1.025 |
| | $4 \times 4$ | 1.000 | 1.001 | 1.000 | 1.005 |
| | $8 \times 8$ | 1.000 | 1.002 | 1.000 | 1.004 |

(c) Response for distorted mesh layouts under concentrated load at the center of the plate (thickness = 0.02)

| Element | Mesh | $\alpha$: simply supported edge | $\alpha$: clamped edge |
|---|---|---|---|
| MITC4 | distort-1 | 0.986 | 0.807 |
| | distort-2 | 0.984 | 0.922 |
| MITC8 | distort-1 | 1.002 | 0.975 |
| | distort-2 | 0.999 | 0.994 |
| MITC7′ | distort-1 | 0.966 | 0.827 |
| | distort-2 | 0.991 | 0.975 |
| MITC9′ | distort-1 | 1.011 | 1.025 |
| | distort-2 | 0.999 | 1.001 |
| MITC7 | distort-1 | 0.965 | 0.844 |
| | distort-2 | 0.991 | 0.978 |
| MITC9 | distort-1 | 1.002 | 1.015 |
| | distort-2 | 0.999 | 1.001 |

† $\alpha = \frac{w^{\text{fem}}}{w^{\text{analyt.}}}$ at center of the plate.

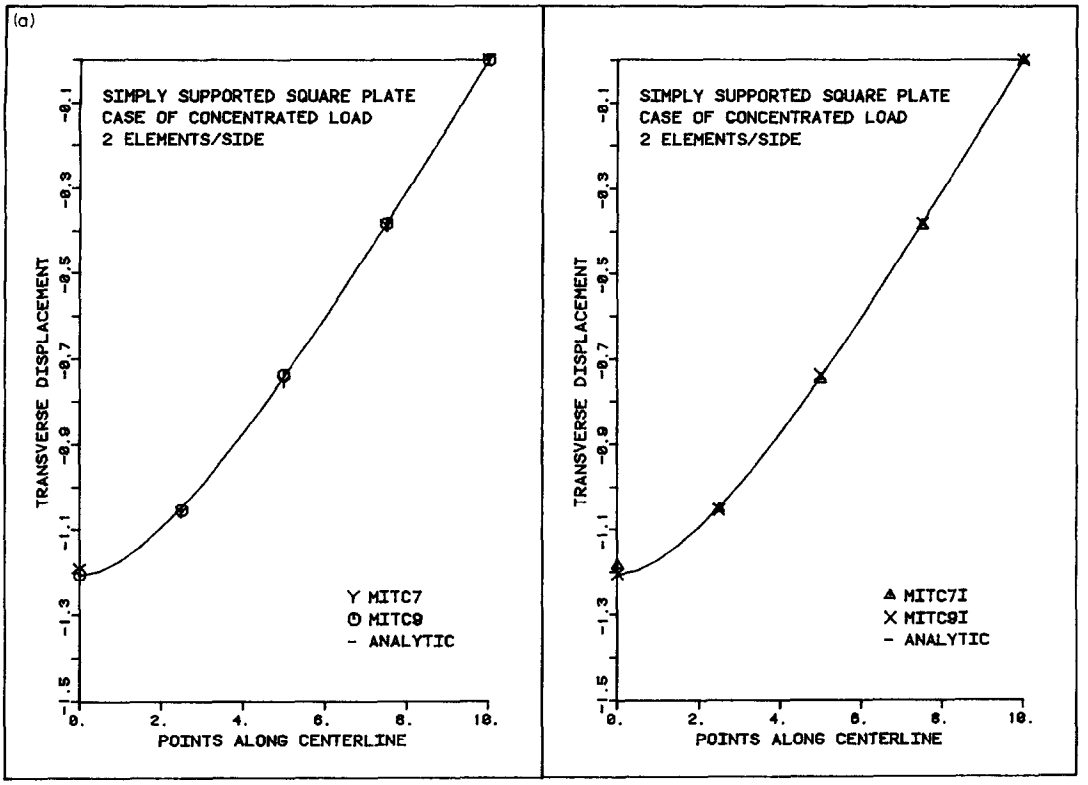
(a)
SIMPLY SUPPORTED SQUARE PLATE
CASE OF CONCENTRATED LOAD
2 ELEMENTS/SIDE
TRANSVERSE DISPLACEMENT
POINTS ALONG CENTERLINE
Y MITC7
O MITC9
- ANALYTIC
SIMPLY SUPPORTED SQUARE PLATE
CASE OF CONCENTRATED LOAD
2 ELEMENTS/SIDE
TRANSVERSE DISPLACEMENT
POINTS ALONG CENTERLINE
Δ MITC7I
X MITC9I
- ANALYTIC

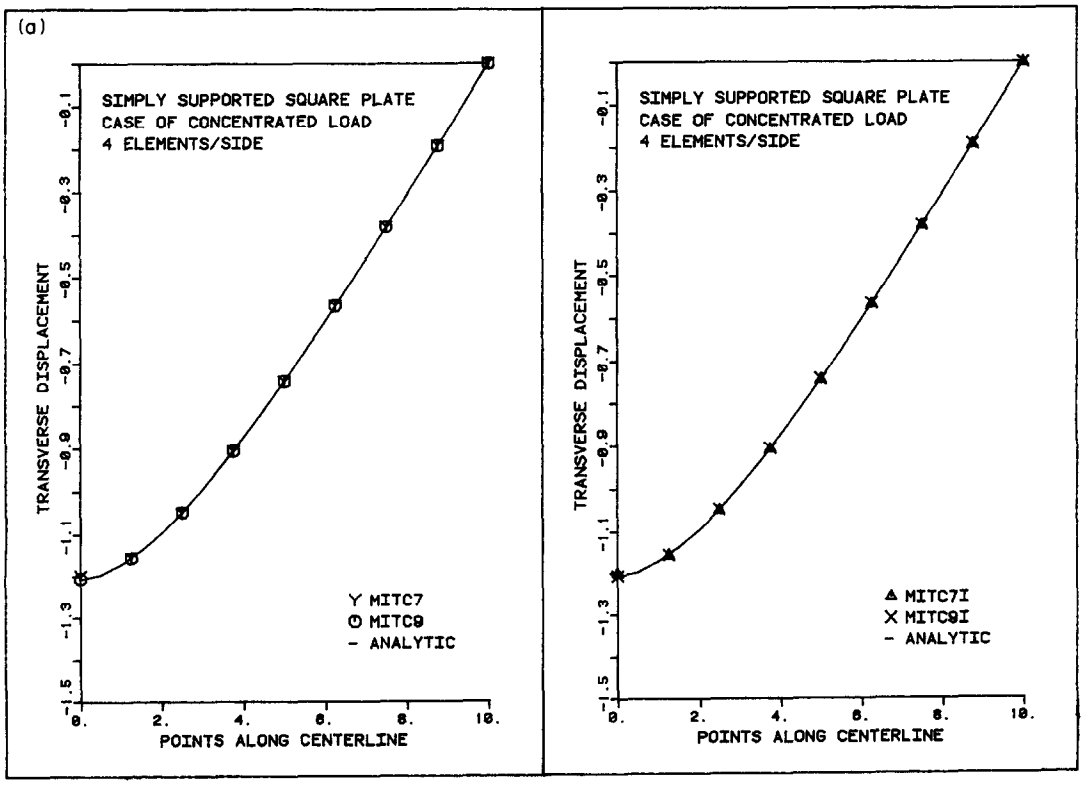
(a)
SIMPLY SUPPORTED SQUARE PLATE
CASE OF CONCENTRATED LOAD
4 ELEMENTS/SIDE
TRANSVERSE DISPLACEMENT
POINTS ALONG CENTERLINE
Y MITC7
O MITC9
- ANALYTIC
SIMPLY SUPPORTED SQUARE PLATE
CASE OF CONCENTRATED LOAD
4 ELEMENTS/SIDE
TRANSVERSE DISPLACEMENT
POINTS ALONG CENTERLINE
Δ MITC7I
X MITC9I
- ANALYTIC

Fig. 6(a)

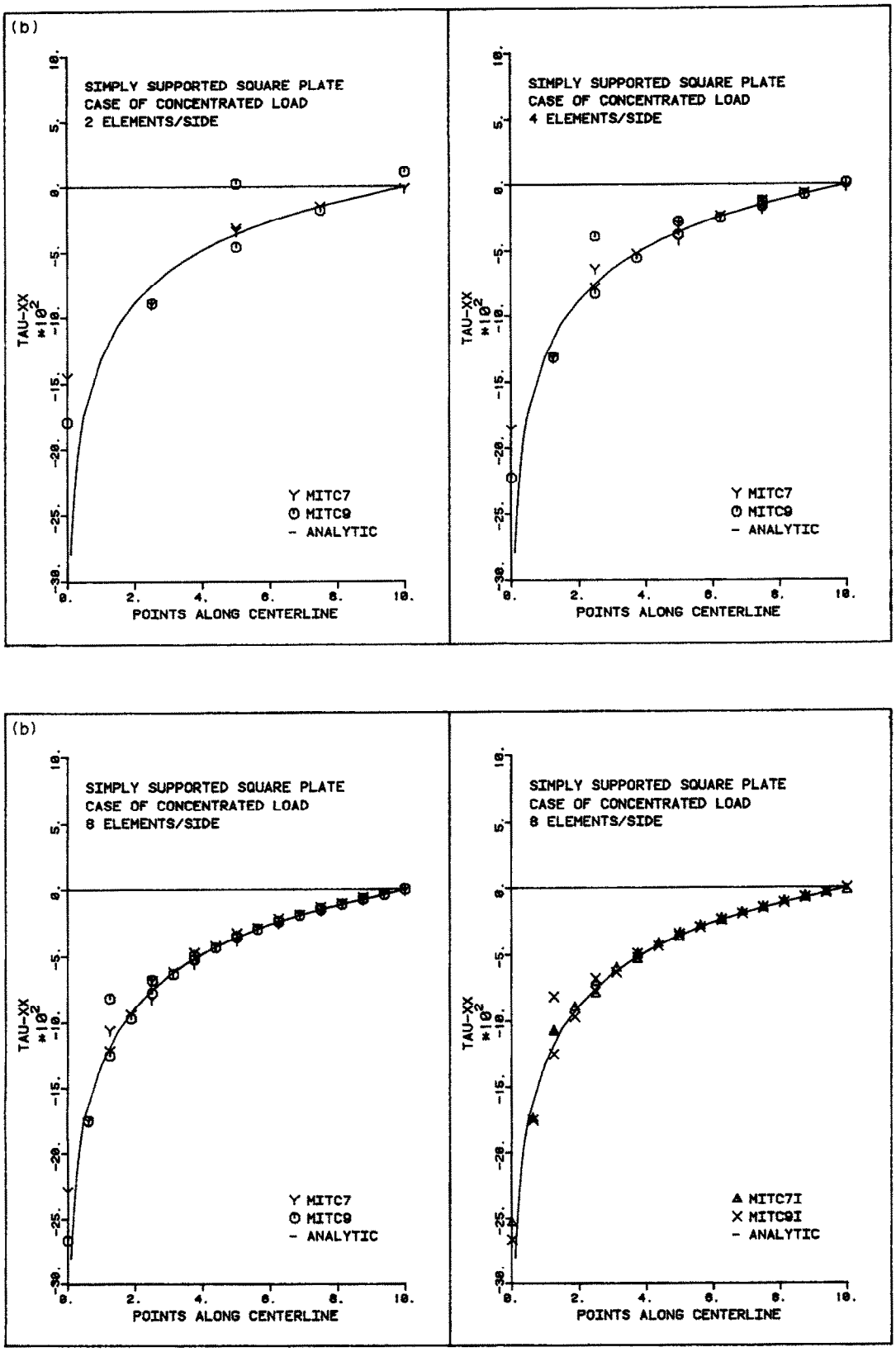
(b)
SIMPLY SUPPORTED SQUARE PLATE
CASE OF CONCENTRATED LOAD
2 ELEMENTS/SIDE
TAU-XX *10^2
POINTS ALONG CENTERLINE
Y MITC7
O MITC9
- ANALYTIC
SIMPLY SUPPORTED SQUARE PLATE
CASE OF CONCENTRATED LOAD
4 ELEMENTS/SIDE
TAU-XX *10^2
POINTS ALONG CENTERLINE
Y MITC7
O MITC9
- ANALYTIC
(b)
SIMPLY SUPPORTED SQUARE PLATE
CASE OF CONCENTRATED LOAD
8 ELEMENTS/SIDE
TAU-XX *10^2
POINTS ALONG CENTERLINE
Y MITC7
O MITC9
- ANALYTIC
SIMPLY SUPPORTED SQUARE PLATE
CASE OF CONCENTRATED LOAD
8 ELEMENTS/SIDE
TAU-XX *10^2
POINTS ALONG CENTERLINE
▲ MITC7I
X MITC9I
- ANALYTIC

Fig. 6(b)

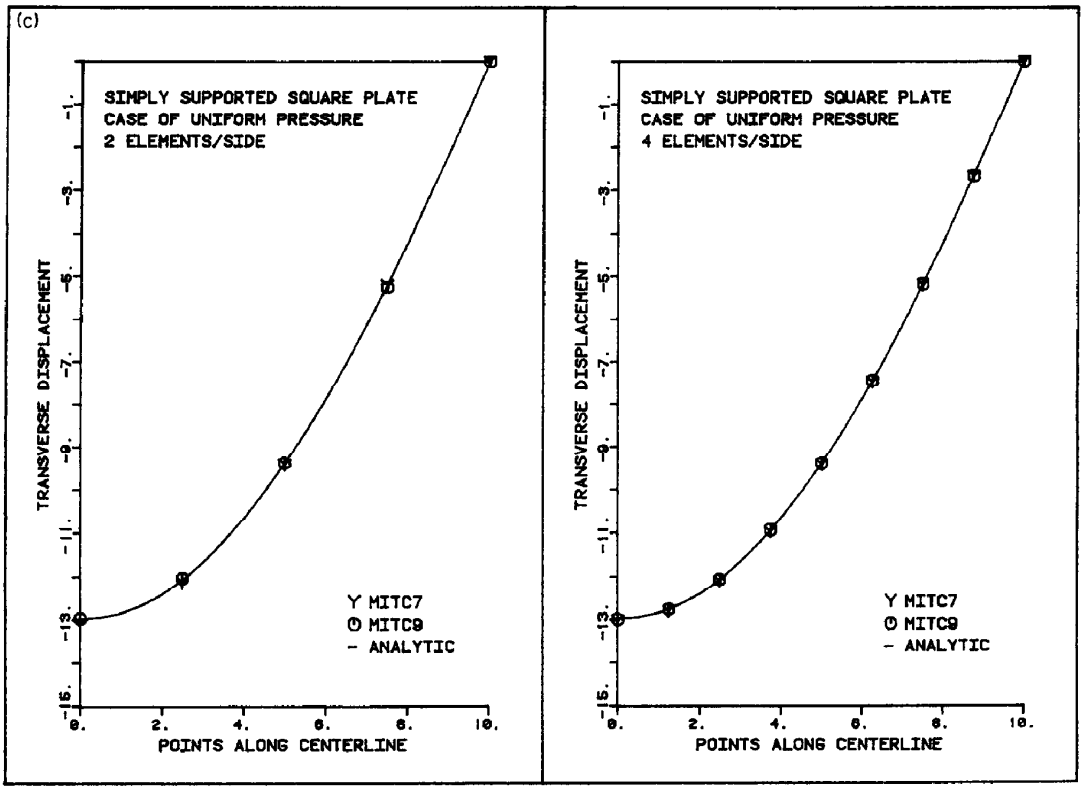
(c)
SIMPLY SUPPORTED SQUARE PLATE
CASE OF UNIFORM PRESSURE
2 ELEMENTS/SIDE
TRANSVERSE DISPLACEMENT
POINTS ALONG CENTERLINE
Y MITC7
MITC9
- ANALYTIC
SIMPLY SUPPORTED SQUARE PLATE
CASE OF UNIFORM PRESSURE
4 ELEMENTS/SIDE
TRANSVERSE DISPLACEMENT
POINTS ALONG CENTERLINE
Y MITC7
MITC9
- ANALYTIC

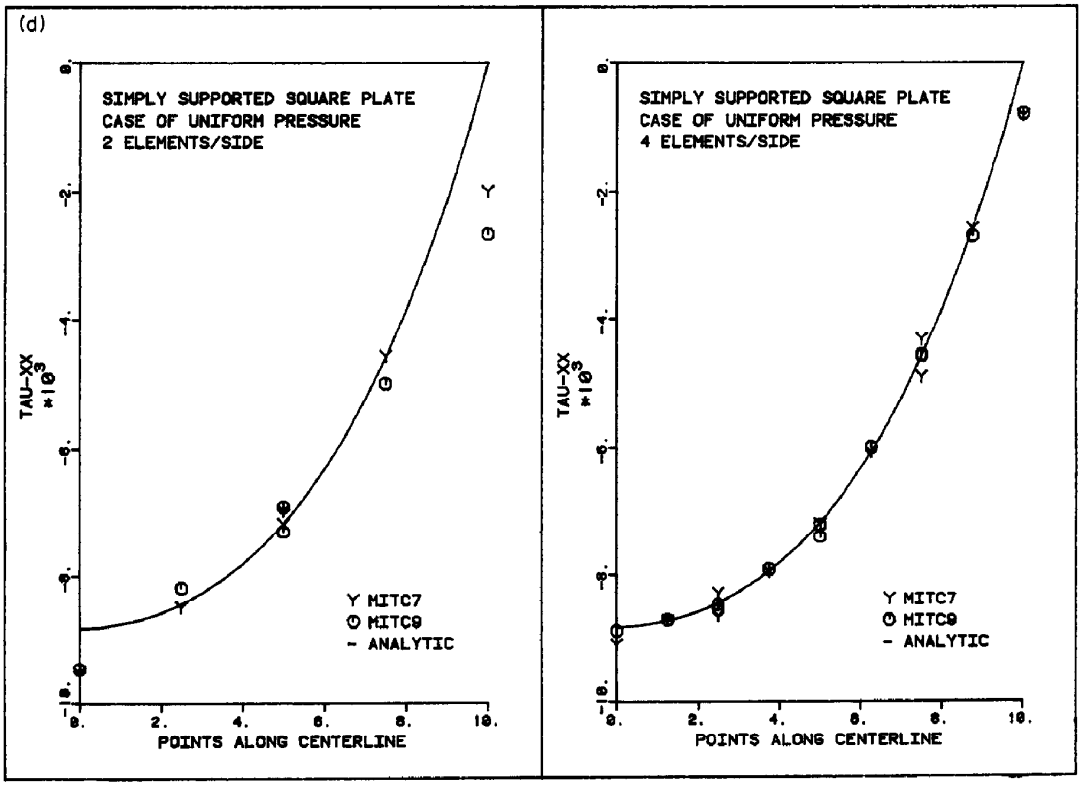
(d)
SIMPLY SUPPORTED SQUARE PLATE
CASE OF UNIFORM PRESSURE
2 ELEMENTS/SIDE
TAU-XX *10^3
POINTS ALONG CENTERLINE
Y MITC7
MITC9
- ANALYTIC
SIMPLY SUPPORTED SQUARE PLATE
CASE OF UNIFORM PRESSURE
4 ELEMENTS/SIDE
TAU-XX *10^3
POINTS ALONG CENTERLINE
Y MITC7
MITC9
- ANALYTIC

Fig. 6(c, d)

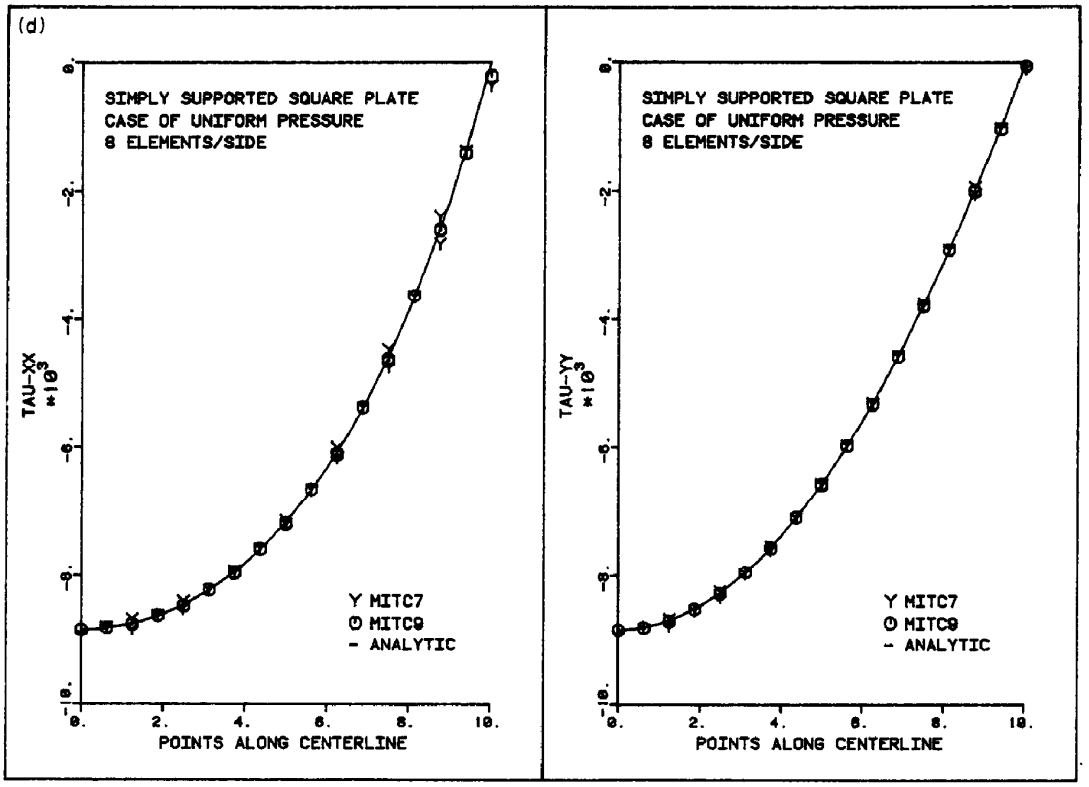


Fig. 6(d)

Fig. 6. Displacement/stress response of a simply supported square plate: meshes of Fig. 5(a)–(d). (a) Transverse displacement along centerline of the plate, case of concentrated load. (b) Stress along centerline of the plate, case of concentrated load. (c) Transverse displacement along centerline of the plate, case of uniform pressure loading. (d) Stress along centerline of the plate, case of uniform pressure loading.

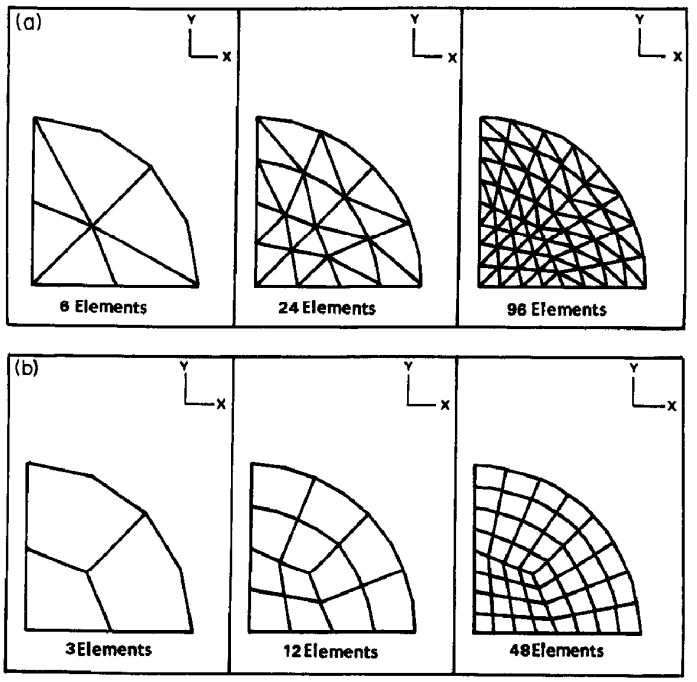


Fig. 7. Finite element meshes used for analysis of a circular plate. Diameter = 20, thickness = 0.02, $E = 2.1 \times 10^6$, $\nu = 0.3$. Due to symmetry only one quarter of the plate is discretized. (a) Mesh layouts using MITC7 elements. (b) Mesh layouts using MITC9 elements.

Table 2. Analysis of a circular plate subjected to concentrated load at the center of the plate. The analytical solution used as reference is the Kirchhoff plate theory solution [13]

| Element | Mesh | α†: simply supported edge | α: clamped edge |
|---|---|---|---|
| MITC4 | 3 elements | 0.983 | 0.786 |
| | 12 elements | 0.995 | 0.948 |
| | 48 elements | 0.998 | 0.986 |
| MITC8 | 3 elements | 0.990 | 0.984 |
| | 12 elements | 0.999 | 0.997 |
| | 48 elements | 1.000 | 0.997 |
| MITC7′ | 6 elements | 1.006 | 0.965 |
| | 24 elements | 1.000 | 0.990 |
| | 96 elements | 1.000 | 0.997 |
| MITC9′ | 3 elements | 0.992 | 0.973 |
| | 12 elements | 0.998 | 0.997 |
| | 48 elements | 1.000 | 1.000 |
| MITC7 | 6 elements | 0.987 | 0.980 |
| | 24 elements | 0.996 | 0.992 |
| | 96 elements | 0.999 | 0.998 |
| MITC9 | 3 elements | 0.997 | 0.991 |
| | 12 elements | 0.999 | 0.998 |
| | 48 elements | 1.000 | 1.000 |

† $\alpha = \frac{w^{\text{fem}}}{w^{\text{analyt.}}}$ at center of the plate (thickness = 0.02).

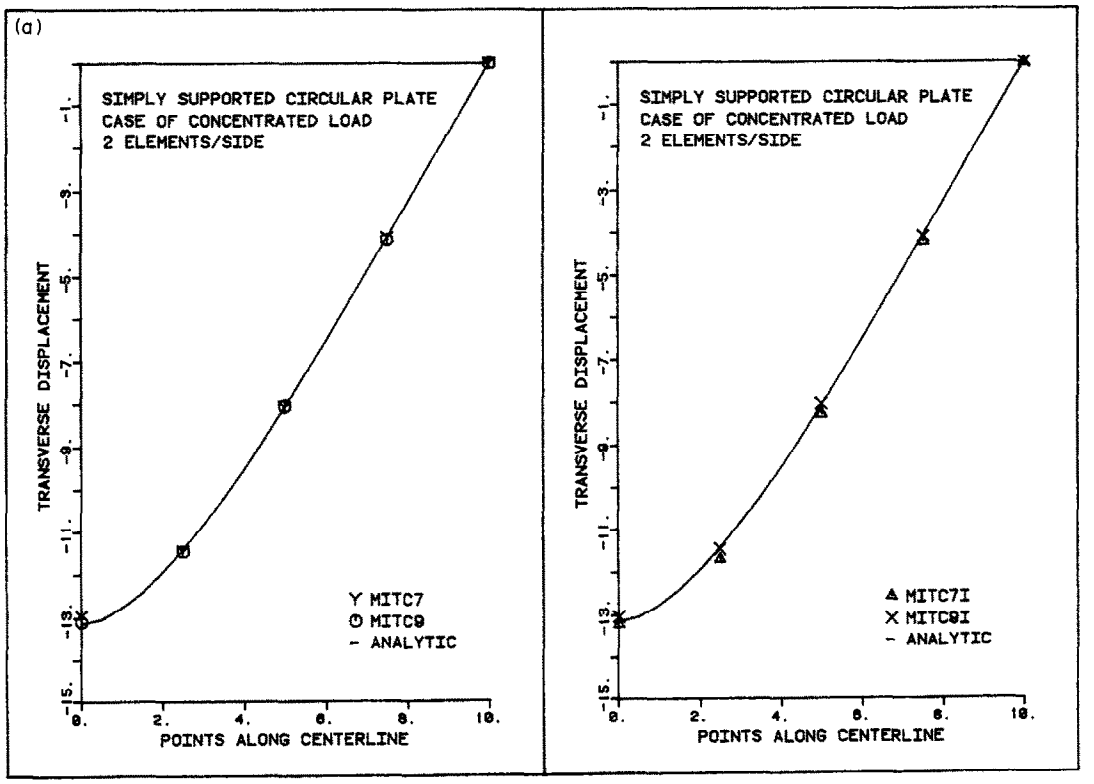


Fig. 8(a)

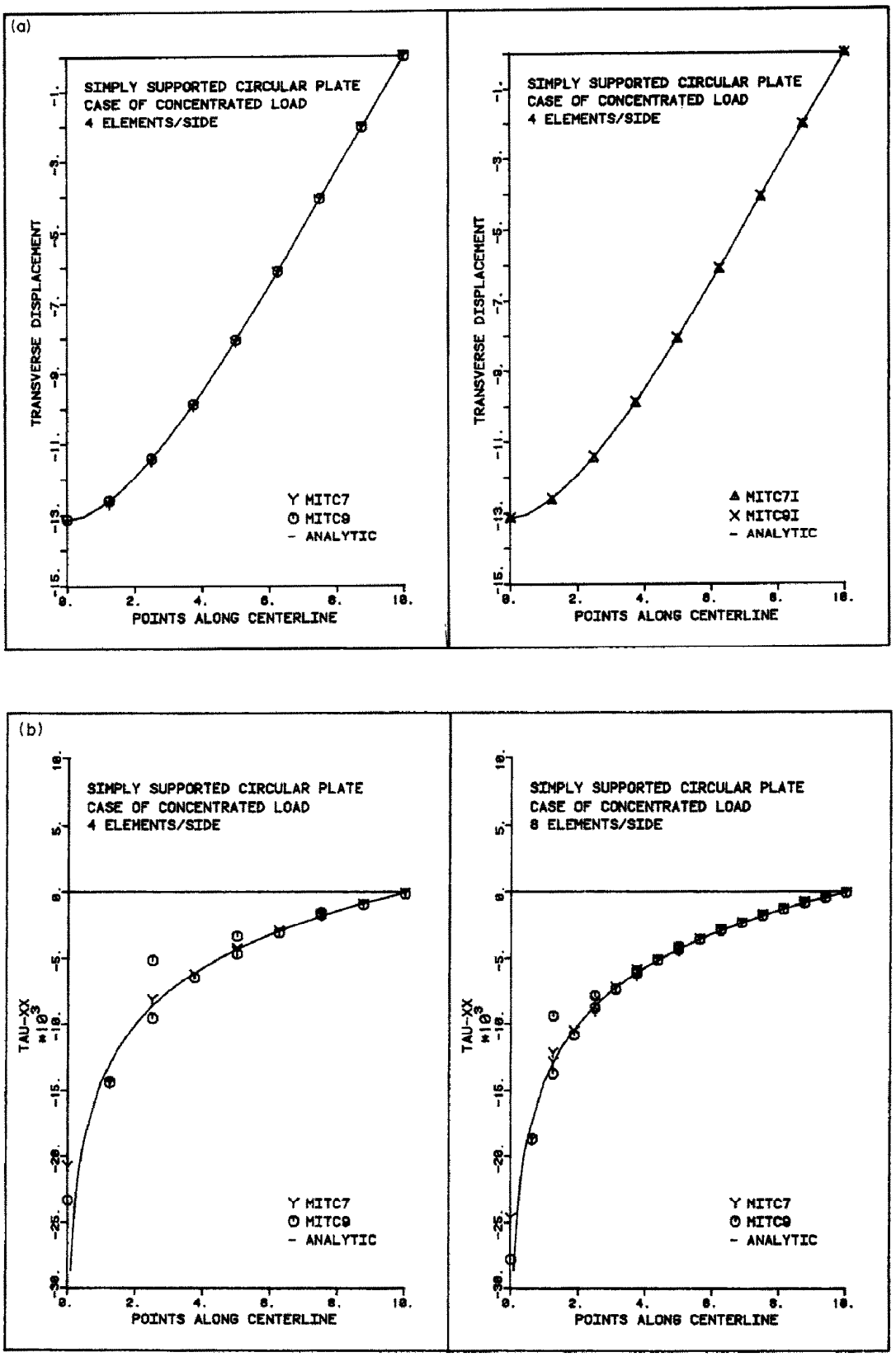
(a)
SIMPLY SUPPORTED CIRCULAR PLATE
CASE OF CONCENTRATED LOAD
4 ELEMENTS/SIDE
TRANSVERSE DISPLACEMENT
POINTS ALONG CENTERLINE
Y MITC7
⊙ MITC9
- ANALYTIC
SIMPLY SUPPORTED CIRCULAR PLATE
CASE OF CONCENTRATED LOAD
4 ELEMENTS/SIDE
TRANSVERSE DISPLACEMENT
POINTS ALONG CENTERLINE
△ MITC7I
X MITC9I
- ANALYTIC
(b)
SIMPLY SUPPORTED CIRCULAR PLATE
CASE OF CONCENTRATED LOAD
4 ELEMENTS/SIDE
TAU-XX *10^3
POINTS ALONG CENTERLINE
Y MITC7
⊙ MITC9
- ANALYTIC
SIMPLY SUPPORTED CIRCULAR PLATE
CASE OF CONCENTRATED LOAD
8 ELEMENTS/SIDE
TAU-XX *10^3
POINTS ALONG CENTERLINE
Y MITC7
⊙ MITC9
- ANALYTIC

Fig. 8(a, b)

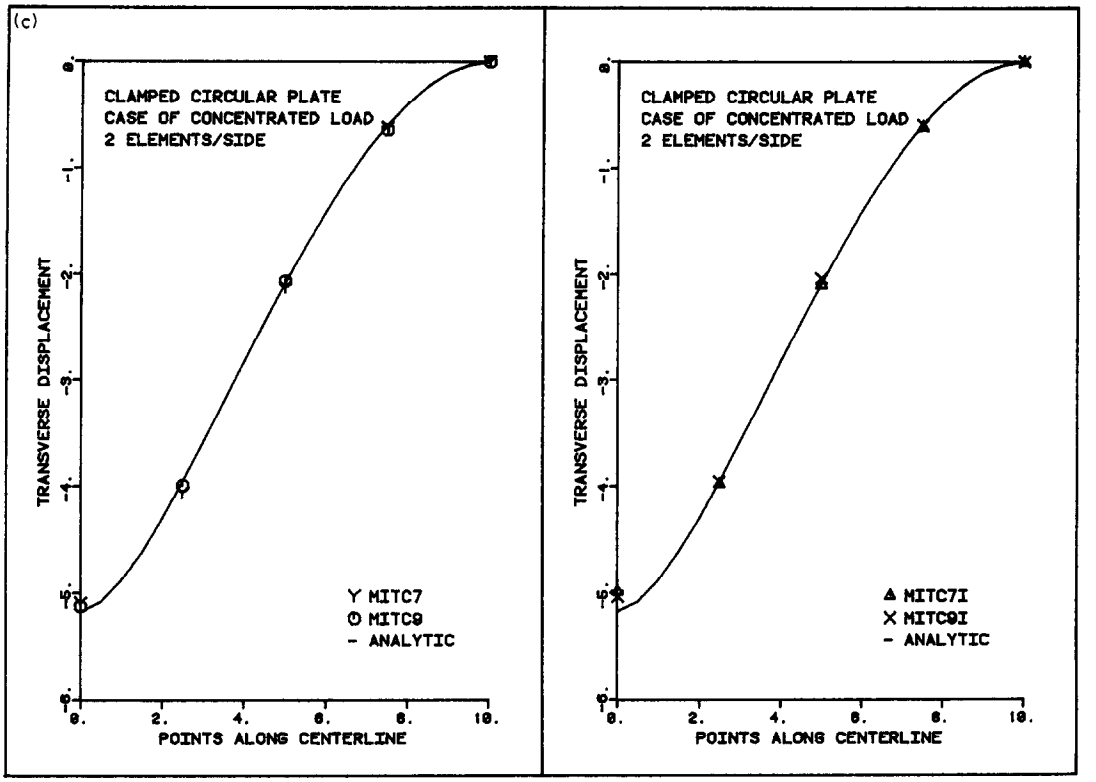
(c)
CLAMPED CIRCULAR PLATE
CASE OF CONCENTRATED LOAD
2 ELEMENTS/SIDE
TRANSVERSE DISPLACEMENT
POINTS ALONG CENTERLINE
Y MITC7
O MITC9
- ANALYTIC
CLAMPED CIRCULAR PLATE
CASE OF CONCENTRATED LOAD
2 ELEMENTS/SIDE
TRANSVERSE DISPLACEMENT
POINTS ALONG CENTERLINE
Δ MITC7I
X MITC9I
- ANALYTIC

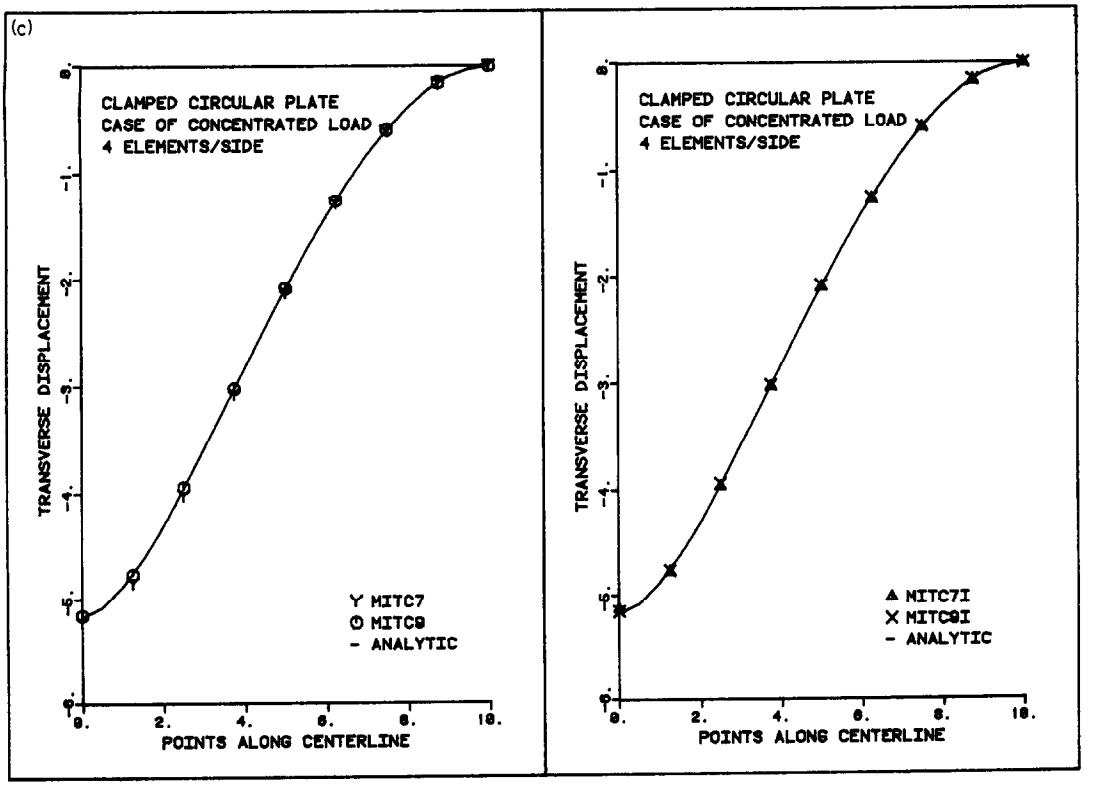
(c)
CLAMPED CIRCULAR PLATE
CASE OF CONCENTRATED LOAD
4 ELEMENTS/SIDE
TRANSVERSE DISPLACEMENT
POINTS ALONG CENTERLINE
Y MITC7
O MITC9
- ANALYTIC
CLAMPED CIRCULAR PLATE
CASE OF CONCENTRATED LOAD
4 ELEMENTS/SIDE
TRANSVERSE DISPLACEMENT
POINTS ALONG CENTERLINE
Δ MITC7I
X MITC9I
- ANALYTIC

Fig. 8(c)

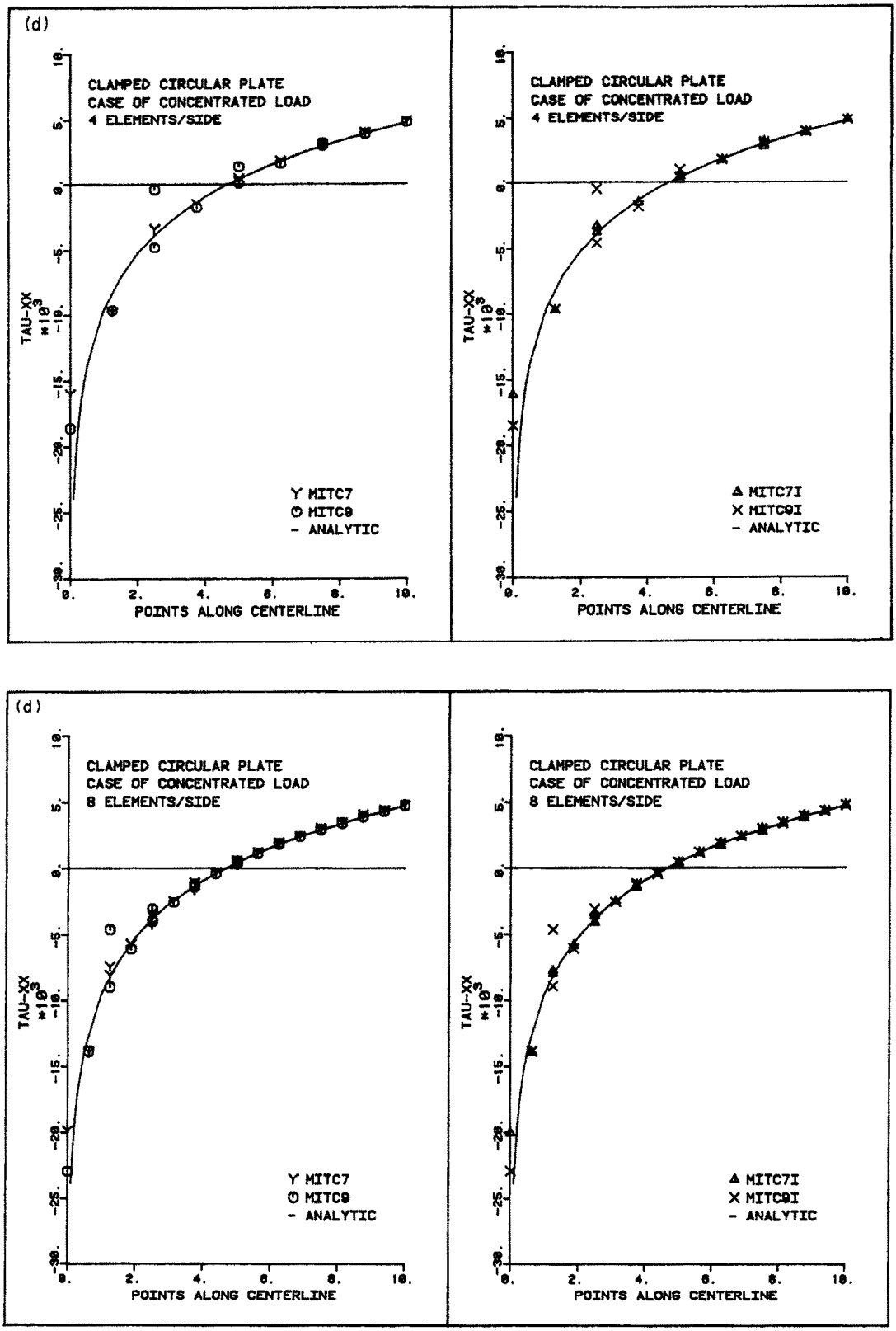


Fig. 8(d)

Fig. 8. Displacement/stress response of a circular plate. (a) Transverse displacement along centerline of the plate, case of simply supported edge. (b) Stress along centerline of the plate, case of simply supported edge. (c) Transverse displacement along centerline of the plate, case of clamped edge. (d) Stress along centerline of the plate, case of clamped edge.

placement and stress distributions calculated using the MITC7 and MITC9 elements. Note that as expected, and as for the analysis of the square plate, the stress jumps at the nodal points are less severe for the fine meshes, and are confined to the area of the stress singularity, i.e. the center of the plate.

As in the analysis of the square plate, there is little difference between the results obtained with the MITC7$^I$ and MITC7 elements, and the MITC9$^I$ and MITC9 elements, respectively.

## 7. CONCLUDING REMARKS

The objective in this paper was to summarize the formulation of the MITC7 and MITC9 plate bending elements and to present numerical results. The elements are based on the Reissner–Mindlin plate theory and a mixed interpolation of the transverse displacement/section rotations and the transverse shear strain components. The strain interpolations are 'tied on the element' to the interpolations of the transverse displacement/section rotations; hence the only final element unknowns are the nodal point transverse displacements and section rotations. The numerical evaluation of these elements shows their high predictive capabilities.

An interesting point is that the mathematical theory used in the formulation of the elements strictly asks for some point-tying and an integral-tying of the assumed transverse shear strain components to the transverse displacement/section rotations. However, our numerical evaluation shows that instead of the integral-tying a point-tying can be used. The numerical results with point-tying are as accurate and for both the triangular and the quadrilateral elements, the point-tying is of course computationally more efficient. The point-tying is also appealing for the development of these plate elements to general linear and nonlinear shell elements.

## REFERENCES

1. E. Dvorkin and K. J. Bathe, A continuum mechanics based four-node shell element for general nonlinear analysis. *Engng Comput.* **1**, 77–88 (1984).
2. K. J. Bathe and E. Dvorkin, A four-node plate bending element based on Mindlin–Reissner plate theory and a mixed interpolation. *Int. J. Numer. Meth. Engng* **21**, 367–383 (1985).
3. K. J. Bathe and E. Dvorkin, A formulation of general shell elements—the use of mixed interpolation of tensorial components. *Int. J. Numer. Meth. Engng* **22**, 697–722 (1986).
4. K. J. Bathe and F. Brezzi, A simplified analysis of two plate bending elements—the MITC4 and MITC9 elements. *Proc. NUMETA Conf.*, University College of Swansea, Wales, July (1987).
5. F. Brezzi, K. J. Bathe and M. Fortin, Mixed-interpolated elements for Reissner–Mindlin plates. *Int. J. Numer. Meth. Engng* (in press).
6. ADINA—a finite element program for automatic dynamic incremental nonlinear analysis. Report ARD 87-1, ADINA R&D, Inc., Watertown, MA (1987).
7. K. J. Bathe and F. Brezzi, On the convergence of a four-node plate bending element based on Mindlin–Reissner plate theory and a mixed interpolation. In *Proceedings, Conference on Mathematics of Finite Elements and Applications V* (Edited by J. R. Whiteman), pp. 491–503. Academic Press, New York (1985).
8. F. Brezzi and K. J. Bathe, Studies of finite element procedures—the Inf–Sup condition, equivalent forms and applications. In *Proceedings, Conference on Reliability of Methods for Engineering Analysis* (Edited by K. J. Bathe and D. R. J. Owen). Pineridge Press, Swansea (1986).
9. P. A. Raviart and J. M. Thomas, A mixed finite element method for second-order elliptic problems. In *Mathematical Aspects of Finite Element Methods*, Lecture Notes in Mathematics, Vol. 606, pp. 292–315. Springer, Berlin (1975).
10. F. Brezzi, J. Douglas Jr., M. Fortin and L. D. Marini, Efficient rectangular mixed finite elements in two and three space variables. *RAIRO MAN* **21**, 581–604 (1987).
11. J. Douglas Jr. and J. E. Roberts, Global estimates for mixed methods for second-order elliptic equations. *Math. Comput.* **44**, 39–52 (1985).
12. T. Sussman and K. J. Bathe, A finite element formulation for nonlinear incompressible elastic and inelastic analysis. *Comput. Struct.* **26**, 357–409 (1987).
13. S. P. Timoshenko and S. Woinowsky-Krieger, *Theory of Plates and Shells*, 2nd Edn. McGraw–Hill (1959).
14. B. Häggblad and K. J. Bathe, Specifications of boundary conditions for Reissner–Mindlin plate bending finite elements. *Int. J. Numer. Meth. Engng* (in review).